

# Multi-boson splashes at future colliders from electroweak compositeness

G. Cacciapaglia<sup>1,2,\*</sup>, A. Deandrea<sup>3,4,†</sup>, A.M. Iyer<sup>5,‡</sup>, S. Kulkarni<sup>6,§</sup> and A.K. Singh<sup>5,¶</sup>

<sup>1</sup>Laboratoire de Physique Théorique et Hautes Énergies (LPTHE), UMR 7589,  
Sorbonne Université & CNRS, 4 place Jussieu, 75252 Paris Cedex 05, France

<sup>2</sup>Quantum Theory Center (QTC) & D-IAS, Southern Denmark Univ., Campusvej 55, 5230 Odense M, Denmark

<sup>3</sup>Université Claude Bernard Lyon 1, CNRS/IN2P3, IP2I UMR 5822, F-69100 Villeurbanne, France

<sup>4</sup>Department of Physics, University of Johannesburg, Box 524, Auckland Park 2006, South Africa

<sup>5</sup>Department of Physics, Indian Institute of Technology Delhi, New Delhi-110016, India

<sup>6</sup>Institute of Physics, NAWI Graz, University of Graz, Universitätsplatz 5, A-8010 Graz, Austria

We propose a new collider signature for the composite origin of the electroweak symmetry breaking of the standard model. The Higgs sector consists of new fundamental fermions (hyper-quarks), which confine at a hadronization scale  $\Lambda_{HC} \sim \text{few TeV}$ . At energies above  $\Lambda_{HC}$ , the Drell-Yan production of the hyper-quarks leads to the production of a few electroweak bosons, in analogy with hadron production in QCD at  $e^+e^- \rightarrow q\bar{q}$  around a few GeV. We show that this regime can be probed at future colliders, namely the proposed 100 TeV hadron collider (FCC-hh) and a 10 TeV muon collider. Together with the direct discovery of electroweak resonances, the multi electroweak boson signature provides a smoking gun for Higgs compositeness.

The origin of the electroweak (EW) symmetry breaking in the Standard Model (SM) remains unresolved. A class of models that aims at providing a dynamical explanation poses the Higgs boson as a bound state within a new composite sector akin to QCD, where spontaneous symmetry breaking arises. A scaled-up version of QCD, dubbed Technicolor (TC), was the first concrete realization [1, 2]. A generic TC-like model consists of a new fundamental fermionic sector (made of hyper-quarks,  $q_{HC}$ ), charged under the EW group and a new confining hypercolor group  $G_{HC}$ . Similarly to QCD, the new dynamics is characterized by a new physics scale  $\Lambda_{HC} \sim \mathcal{O}(\text{few}) \text{ TeV}$ , where  $q_{HC}$  bound states are present. In this setup, the longitudinal polarization of the EW bosons and the Higgs emerge as light resonances below  $\Lambda_{HC}$ .

If the  $q_{HC}$  condensate breaks the EW symmetry, then one would naturally expect  $\Lambda_{HC} \sim 1 - 3 \text{ TeV}$ . There are models where the condensate also features an EW-preserving direction, and the EW symmetry breaking is due to misalignment [3], hence allowing for larger  $\Lambda_{HC}$  up to tens of TeV. In those models, the Higgs boson emerges as a pseudo-Goldstone, while a TC-like direction can always be reached continuously [4]. The scale  $\Lambda_{HC}$  serves as an indicator beyond which the composite theories can be treated in terms of the fundamental hyper-quarks and hyper-gluons and beyond the chiral approximation. Investigations for compositeness at past and current colliders, such as the Large Electron-Positron (LEP) and the Large Hadron (LHC) colliders, have been focused either on precision measurements in the EW sector (gauge and Higgs couplings) or on searches for individual resonances. This strategy was mainly due to the limited energies in the individual collision, reaching up to a few TeV at partonic level. This work sketches out a novel strategy for the exploration of TC-like theories at future higher energy colliders, where large multiplicities of composite resonances are produced.

The exploration of strongly-interacting theories at colliders can be classified into regimes that depend on the available collision energy, as parametrized by partonic Mandelstam variable  $\hat{s}$ . For  $\sqrt{\hat{s}} < \Lambda_{HC}$ , chiral expansion is used to study the direct production of a small (one or two) number of light resonances. For  $\sqrt{\hat{s}} > \Lambda_{HC}$ , instead, the production of resonances can be parametrized in terms of perturbative matrix elements involving hyper-quarks and hyper-gluons. Hence, irrespective of the theory, whether QCD or TC-like, the corresponding regimes can be conveniently quantified by the ratio  $\sqrt{\hat{s}}/\Lambda$ . In the case of QCD, the inclusive measurement for  $e^+e^- \rightarrow \text{multi-mesons}$  is consistent with the evaluations from the perturbative matrix element  $\mathcal{M}(e^+e^- \rightarrow q\bar{q})$  at energies above  $\sim 2 \text{ GeV}$ . The mesons are formed from the outgoing quarks by a process of fragmentation and hadronization [5, 6]. Depending on the number of produced mesons, the value of  $\sqrt{\hat{s}}/\Lambda_{QCD}$  can further classify the perturbative regime into two broad categories:

- i)  $\sqrt{\hat{s}}/\Lambda_{QCD} \sim \mathcal{O}(1 - 10)$  leads to the production of a small number of mesons (process  $2 \rightarrow \text{few}$ ). In this regime, data is described in terms of  $R$ -ratios [7–9].
- ii)  $\sqrt{\hat{s}}/\Lambda_{QCD} \gg \mathcal{O}(10)$  leads to  $2 \rightarrow \text{many}$  mesons, with the final states characterized in terms of QCD-jets rather than explicit meson multiplicities. An example is collisions at the Z-pole at LEP [10, 11].

Although the boundary between  $2 \rightarrow \text{few}$  and  $2 \rightarrow \text{many}$  regimes is not well defined, this classification helps define the final state. A similar framework can be used in TC-like theories. The analogue of QCD-mesons ( $\pi$ 's etc.) are ‘EW-bosons’, i.e. the lightest bound states of the hyper-quarks. They are identified as (pseudo-)scalars that are not charged under QCD’s  $SU(3)$  and have masses around the EW scale. The ‘EW-bosons’ include the longitudinal components of the massive gauge

bosons and the Higgs, together with other spin-0 states, whose number and properties depend on the global symmetry of the specific TC-like model. If we consider a benchmark  $\Lambda_{HC} = 2$  TeV, the regime  $2 \rightarrow few$  would occur if  $\sqrt{\hat{s}} \sim 10$  TeV. On the other hand,  $\sqrt{\hat{s}} \gtrsim 50$  TeV would be necessary for the realization of the  $2 \rightarrow many$  regime. While the latter is beyond the reach of any foreseeable terrestrial accelerator, the former regime with  $\sqrt{\hat{s}} \sim 10$  TeV can be reached at the proposed 100 TeV hadron collider (FCC-hh) [12] and at a high-energy muon collider [13].

In this letter, we present a proof-of-principle study of  $2 \rightarrow few$  EW-boson process in TC-like theories at future high energy colliders. The pair production  $pp(q\bar{q}')/\mu^+\mu^- \rightarrow q_{HC}\bar{q}'_{HC}$ , followed by fragmentation and hadronization under  $G_{HC}$ , is treated as the analogue of  $e^+e^- \rightarrow q\bar{q}$  in QCD at low-energy colliders. In both cases, the hadronizing quarks are produced via their EW interactions. We show that such a multi EW-boson final state yields characteristic kinematic properties, which allow for a clear distinction from purely SM processes. This signature, together with the direct discovery of light resonances (produced singly or in pairs), provides a smoking gun for the discovery of composite dynamics in the Higgs sector.

For concreteness, we consider a strong dynamics as close as possible to that of QCD, hence  $G_{HC} = SU(N)_{HC}$  with  $q_{HC}$  in the fundamental representation.<sup>1</sup> In the most minimal model, the hyper-quarks are organized into doublets under the global flavor symmetry  $G_F \equiv SU(2)_L \times SU(2)_R$ :

$$q_{HC} \equiv \begin{pmatrix} U \\ D \end{pmatrix}_L \oplus \begin{pmatrix} U \\ D \end{pmatrix}_R. \quad (1)$$

The flavor symmetry is partly gauged by the EW symmetry  $G_{EW} = SU(2)_L \times U(1)_Y$ . These fields transform under  $SU(N)_{HC} \times G_{EW}$  as follows:

$$\begin{pmatrix} U \\ D \end{pmatrix}_L \equiv (N, 2, y), \quad U_R \equiv (N, 1, y + \frac{1}{2}), \quad D_R \equiv (N, 1, y - \frac{1}{2}).$$

At a scale  $\Lambda_{HC}$ , the formation of a hyper-quark condensate,

$$\langle \overline{U}_L U_R \rangle = \langle \overline{D}_L D_R \rangle \neq 0, \quad (2)$$

is responsible for the breaking of the flavor symmetry to its diagonal subgroup,  $G_F \rightarrow H \equiv SU(2)_V$ . In this minimalist construction, the three Goldstone bosons are identified with the longitudinal components of the  $W^\pm$

and  $Z$  gauge bosons, while the analogue of the CP-even  $\sigma$  meson can be identified with the Higgs boson [16–19]. Instead of identifying individual bosons, we label all mesons as EW-gauge bosons to remain model agnostic. Note that, for  $N = 2$  ( $y = 0$ ), this model corresponds to the ultra-minimal Technicolor of [20], which also allows to embed the Higgs as a pseudo-Goldstone boson [4, 21] thanks to an enhanced global symmetry. Instead,  $N = 3$  ( $y = 1/6$ ) leads to the old-school Technicolor [1, 2], where a light  $\sigma$ -Higgs can be obtained via the addition of heavy TC-quark flavors [22, 23]. Furthermore, top partial compositeness [24] can also be implemented by means of the same heavy flavors [25]. Finally,  $N = 4$  models have also been considered within the framework of partial compositeness in [26, 27]. Models with extended global symmetries can also be constructed, leading to the presence of additional light EW-bosons [28, 29] that will decay predominantly into pairs of EW gauge bosons or third generation fermions [27, 30]. In some models, the EW-bosons may include a dark matter candidate [31–35], hence leading to missing energy in the decay. In the following we only consider TC-like models, where  $\Lambda_{HC}$  is closely related to the EW scale via the meson decay constant  $f_\pi \sim \frac{\sqrt{N}}{4\pi} \Lambda_{HC}$ , with  $f_\pi \equiv v = 2m_W/g$ . In models where the Higgs emerges as a pseudo-Goldstone, a hierarchy between  $f_\pi$  and  $v$  is necessary, with typically  $v/f_\pi \lesssim 0.1$  [36, 37], hence leading to values of  $\Lambda_{HC}$  too large to be accessible at future colliders in the  $2 \rightarrow few$  regime.

For the collider signatures, we consider Drell-Yan production of hyper-quark pairs for both the FCC-hh and muon colliders as follows:

- A)  $pp \rightarrow q_{HC}\bar{q}_{HC}$  and
- B)  $\mu^+\mu^- \rightarrow q_{HC}\bar{q}_{HC}$ .

The processes are simulated using MADGRAPH [38] and PYTHIA [39] at 100 TeV and 10 TeV center-of-mass energy, respectively. The production is due to EW gauge bosons, following the quantum numbers specified above (for  $y = 0$ ). After hadronization, the outgoing EW-bosons are required to be in the central region of the detector, satisfying a pseudo-rapidity cut  $|\eta| < 2.5$ . In the minimal set-up, the final state bosons will be composed of the longitudinal components of the gauge bosons,  $W^\pm$  and  $Z$ . In the extended set-ups, other bosons in the electroweak coset  $G_F/H$ , will also be formed. Other heavy resonances, with masses around  $\Lambda_{HC}$  will also be produced during hadronization, such as spin-1 TC- $\rho$  mesons.

Several parameters govern the properties of the signal in our model, e.g., the multiplicity, phase-space distributions of the EW-bosons. They correspond to the process of fragmentation as well as hadronization, as implemented in the PYTHIA HV module [40, 41]. Among those

<sup>1</sup> Our discussion is also applicable to larger number of flavors and colors, as long as the fermion multiplicity falls below the conformal window [14]. Beyond this regime, simulating the so called near-conformal theories need new developments in Pythia [15].

are `ProbVector`,  $a_L, b_L, r_Q, \sigma_{m_q}$  – parameters that control the hadronization – and  $\Lambda_{HC}$  together with the order of running coupling – parameters that control fragmentation or shower [42]. We chose to investigate a subset of these parameters, which have the largest impact on the signal properties. `ProbVector` controls the probability for a formed meson to be a  $\rho$ , as it ranges from 0 to 1, and its value should be fitted from data. As we are close to the chiral limit,  $m_\pi \ll m_\rho$ , the value for this parameter cannot be easily fixed [43]. We use the QCD template value 0.3, while noting that its increase reduces the scalar mesons multiplicity in the final state. The decay,  $\rho \rightarrow \pi\pi$  could also further enrich the pion multiplicity, however in realistic models other decay channels are also open, rendering the final state model dependent, even in the most minimal model [44–46]. Hence, in our analysis, we conservatively ignore them and only count the scalar states directly produced via the hadronization. We also concentrate on  $a_L, b_L$ , which are two dimensionless parameters entering the Lund fragmentation function [47, 48]. Given the absence of data for TC-like models, the values of the Lund parameters are chosen to be the same as the values recommended for QCD ( $a_L = 0.3$ , and  $b_L = 0.087$ ) [43]. The constituent quark mass is set to  $\Lambda_{HC}$ . The supplementary material provides further insights on the dependence of the results on these parameters. The length of shower is controlled by the ratio  $\sqrt{\hat{s}}/\Lambda_{HC}$  and thus it is an important parameter in determining the final-state EW-boson multiplicity. This

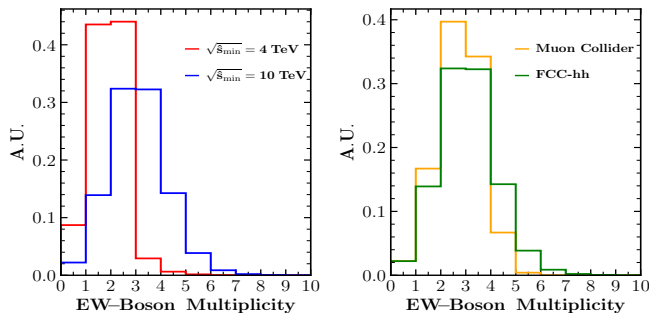


FIG. 1: Final state EW-boson multiplicity.

**Left:** Distribution at FCC-hh for  $\sqrt{\hat{s}_{min}} = 4$  TeV (red) and  $\sqrt{\hat{s}_{min}} = 10$  TeV (blue). **Right:** Comparison between the FCC-hh at  $\sqrt{\hat{s}_{min}} = 10$  TeV (green) and a muon collider at fixed  $\sqrt{\hat{s}} = 10$  TeV (orange)

is illustrated in the left plot of Fig. 1, where the meson multiplicity for a minimum partonic collision energy  $\sqrt{\hat{s}_{min}} = 4(10)$  TeV (red, blue curves) is shown for fixed  $\Lambda_{HC} = 2$  TeV. As the constituent quark mass is set to  $\Lambda_{HC}$ , the kinematics for the Drell-Yan production automatically ensures that the minimum invariant mass is  $\sqrt{\hat{s}_{min}} = 4$  TeV. At this point, no shower is initiated, and

hence the corresponding distribution (red curve) peaks at two bosons. On the other hand,  $\sqrt{\hat{s}_{min}} = 10$  TeV allows for a perturbative  $q_{HC}\bar{q}_{HC}$  production process, followed by shower and hadronization, resulting in larger multiplicities. This is reflected in the blue curve where the boson multiplicity peaks at three. The tail of the distribution as seen in Fig. 1 results from variation of partonic center-of-mass energy  $\sqrt{\hat{s}} > \sqrt{\hat{s}_{min}}$ , in a  $pp$  system. The corresponding plot for the muon collider, operating at a fixed  $\sqrt{\hat{s}}$ , has a significantly suppressed tail. The right plot of Fig. 1 quantifies this statement by comparing the expected EW-boson multiplicity for FCC-hh and muon colliders.

The signal, with a desired multiplicity of final state bosons, has an irreducible SM background of the form  $pp(\mu\mu) \rightarrow XY, XYZ$ , where  $X, Y, Z \equiv$  EW bosons ( $W^\pm, Z$ ). The higher multiplicity final states in the background are primarily due to pair production of off-shell EW bosons and their eventual decay into multi-body final states. The background cross sections are evaluated at leading order from MADGRAPH [38] and PYTHIA [39] by requiring that each of the EW-boson in the final state satisfies  $|\eta| < 2.5$ . The signal cross sections are estimated by factoring the Drell-Yan cross-section ( $\sigma(pp/\mu\mu \rightarrow q_{HC}\bar{q}'_{HC})$ ) with the corresponding efficiency for the three and four body final state. These cross sections can be estimated for different multiplicity of final states. For illustration we consider  $\Lambda_{HC} = 2$ . For three boson EW-bosons final state, signal cross-sections are,  $\sim 64$  ab at FCC-hh with  $\sqrt{\hat{s}_{min}}/\Lambda_{HC} = 5$  and  $\sim 758$  ab at the muon collider with  $\sqrt{\hat{s}}/\Lambda_{HC} = 5$ . The corresponding values for the background, are  $\sim 422$  and  $\sim 4701$  ab, respectively. The numbers for the four boson final state can also be similarly estimated and reflect similar patterns of hierarchy between the signal and the background.

It is interesting to note that the signal and SM cross sections are roughly of the same order of magnitude. This paints a highly optimistic scenario for a potential discovery of a multi EW-boson final state due to fragmentation. This situation is further bolstered by comparing the transverse momentum ( $p_T$ ) distribution of all the EW-bosons for both the signal, with  $\Lambda_{TC} = 2$  TeV, and background. Choosing  $\sqrt{\hat{s}_{min}}/\Lambda_{HC} = 5$  for FCC-hh and  $\sqrt{\hat{s}}/\Lambda_{HC} = 5$  for the muon collider, the distribution is shown in Fig. 2. The top and bottom plots correspond to the FCC-hh and muon collider, respectively. All the EW-bosons from the signal have consistently higher  $p_T$ , as they emerge from the fragmentation of the (heavy) hyper-quarks and are predominantly produced in the transverse plane. On the other hand, the EW-bosons from the background have a tendency to be in the forward direction, and typically only one of the total of three and four bosons in the final state is boosted. Thus, the signal event rate in the higher  $p_T$  bins is expected to be at least comparable with the background. The  $p_T$  dis-

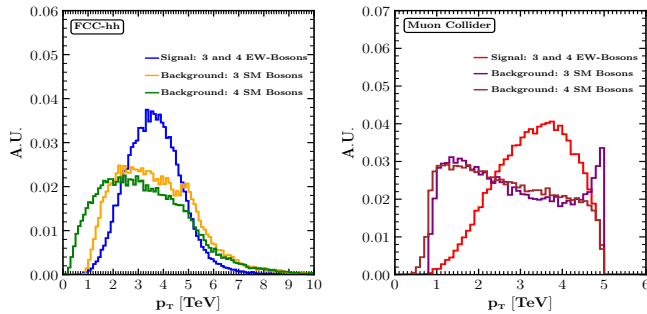


FIG. 2: Leading  $p_T$  distribution of the EW-bosons (signal), and the three and four SM bosons for FCC-hh(left) and muon collider(right).

tribution for the FCC-hh has a smoother longer tail as larger values of partonic center-of-mass energy is accessible. On the other hand, the distribution for the muon collider exhibits a sharp cut-off at 5 TeV as it is operated at a fixed center of mass energy of 10 TeV.

Hence, the ratio  $\sqrt{\hat{s}}/\Lambda$  plays a crucial role in the ability to identify a signal over the background. While higher values of the ratio  $\sqrt{\hat{s}}/\Lambda$  would lead to higher  $p_T$  bosons and higher multiplicity of final states for the signal, one would be limited by a falling cross-section for the signal. As an illustration, Table I shows the cross sections at FCC-hh after cuts for  $\Lambda_{HC} = 2$  TeV and three different values of the ratio,  $\sqrt{\hat{s}_{min}}/\Lambda = 5, 10, 15$ . We also remark that for fixed  $\sqrt{\hat{s}_{min}}/\Lambda$ , the cross-sections decrease with increasing  $\Lambda_{HC}$  and grow linearly with  $N$ .

$\sqrt{\hat{s}_{min}}$ (TeV)	3 Bosons		4 Bosons	
	$\sigma_{SM}$ (ab)	$\sigma_{sig}$ (ab)	$\sigma_{SM}$ (ab)	$\sigma_{sig}$ (ab)
10	422.3	64.7	96.6	29.0
20	13.8	0.8	4.8	1.0
30	0.75	0.01	0.4	0.0

TABLE I: Comparison of SM ( $\sigma_{SM}$ ) and signal ( $\sigma_{sig}$ ) cross sections for  $\Lambda_{HC} = 2$  TeV at FCC-hh. Three and four boson final state are shown at three different  $\sqrt{\hat{s}_{min}}$ .

The extent in  $\Lambda_{HC}$  to which a given signal can be discriminated over the background can be quantified using the binned sensitivity [49]  $Z = \sqrt{\sum_{i=1}^M \left( 2(s_i + b_i) \log \left[ 1 + \frac{s_i}{b_i} \right] - 2s_i \right)}$ , where the sum runs over the bins for a given discriminating variable and  $s_i$  ( $b_i$ ) is the expected number of signal (background) events in the  $i^{th}$  bin at a given luminosity. As  $p_T$  is identified as a useful variable to discriminate signal over background, we calculate the  $Z$ -score using the  $p_T$  distributions with bins of size 20 GeV over the range  $[0, 10]$  TeV. As the study is meant to be a proof-of-principle, the EW bosons for both the signal and background are consid-

ered as final-state objects. As a result, the  $Z$  value corresponds to the maximum possible sensitivity that can be achieved for a given  $\Lambda_{HC}$ . Fig. 3 illustrates the sen-

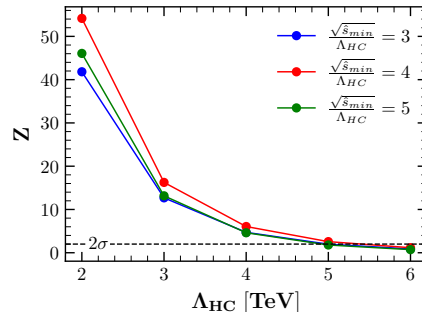


FIG. 3: Variation of the  $Z$ , signal sensitivity with  $\Lambda_{HC}$  for fixed  $\sqrt{\hat{s}_{min}}/\Lambda_{HC}$  ratio.

sitivity  $Z$  for three and four EW-boson final state as a function of  $\Lambda_{HC}$  at FCC-hh, for three different  $\sqrt{\hat{s}_{min}}/\Lambda$  settings/benchmarks. For a given value of  $\Lambda_{HC}$ , an interesting hierarchy in  $Z$  between the three different values of  $\sqrt{\hat{s}_{min}}/\Lambda$  emerges. This is because  $\sqrt{\hat{s}_{min}}/\Lambda = 4$  has the maximum cross section for three and four boson final state. For  $\sqrt{\hat{s}_{min}}/\Lambda = 5$  on the other hand, a higher multiplicity of final states is preferred. The  $2\sigma$  line illustrates the extent to which a bound on  $\Lambda_{HC}$  can be achieved using this methodology. The prospects for a muon collider are relatively less stringent and only  $\Lambda_{HC}$  up to 3 TeV can be excluded at 95% with this method.

In a complete analysis, the identification of each boson will be performed through its decay products. As the signal EW bosons are highly boosted, their decay products will likely be concentrated in a small angular region and hence can be classified as jets. Fig. 4 illustrates the distributions of EW bosons (green dots) in the  $\eta - \phi$  plane for two representative events for the signal with  $\Lambda_{TC} = 2$  TeV. The region enclosed by the red boundary around each boson represents the circular disc with radius  $R < 1$ . This indicates the fact that the eventual decay products of the EW bosons will be distributed over a small region and hence identified as boosted jets. The right plot is particularly interesting as it suggests the clustering of two EW bosons in a single jet, which is extremely rare in the SM. The high values of  $\Lambda_{HC}$  and the available energies favor the exploitation of three and four EW boson final states. However, probing higher values of  $\sqrt{\hat{s}_{min}}/\Lambda_{HC}$  may lead to higher multiplicities, particularly for relatively low values of  $\Lambda_{HC}$ . For example,  $\Lambda_{HC} = 2$  TeV and  $\sqrt{\hat{s}_{min}}/\Lambda_{HC} = 10$ , can lead to about 25 signal events that contain five EW-boson events. Although this does not seem significant, it must be remembered that it may be associated with negligible backgrounds. Higher multiplicities of EW bosons may also derive from non-minimal models, where the cosets

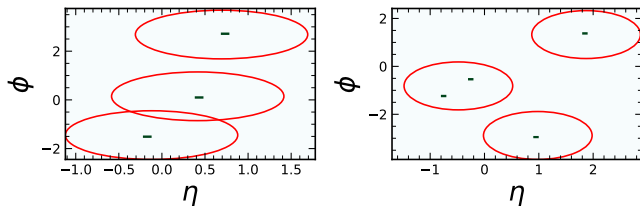


FIG. 4: Visualization of signal in the form of jets with  $R = 1$  and represented by closed red contours.

contain additional light scalars in addition to longitudinal  $W$ ,  $Z$ , and Higgs [29, 30, 50, 51], and from the decays of the  $\rho$  mesons produced via hadronization. The new scalars could decay into a pair of EW gauge bosons (including the photon), hence providing a new handle into this process. A detailed analysis would crucially depend on the specific model, and it is left for future investigations.

Learning from QCD, we explored a novel regime for models of composite Higgs sectors, corresponding to energies a few times larger than the resonance scale  $\Lambda_{HC}$ . In this regime, the effects of the new strong dynamics can be described in terms of Drell-Yan production of the fundamental hyper-quarks, followed by fragmentation and hadronization. We showed that for low values of  $\Lambda_{HC}$  in the few TeV range, a future 100 TeV hadron collider (FCC-hh) and a 10 TeV muon collider provide a picture similar to the one of a few GeV lepton collider for QCD. Higgs compositeness reveals itself by the production of few EW-bosons ( $W$ ,  $Z$  and Higgs), which can be kinematically distinguished from the pure standard model backgrounds. We provide a first proof-of-principle toward the discovery of this regime of TeV-scale strong interactions. This signature provides a clear proxy for the composite nature of the Higgs sector of the standard model and for the dynamical origin of the electroweak symmetry breaking, together with the further direct search for EW-resonances.

#### ACKNOWLEDGMENTS

We thank Nishita Desai for useful discussions and collaboration in the initial phase of the project. We would like to thank MITP for hosting “The Future of Fundamental Composite Dynamics: Theory, Colliders, Cosmology, and Tools”, where many aspects of the project took shape and were discussed. S.K. is supported by the Austrian Science Fund research teams grant STRONG-DM (FG1) and project number P 36947-N. A.M.I. acknowledges the generous support by SERB India through project no. SRG/2022/001003. A.M.I. also thanks the French Institute- Embassy of France in India for facili-

tating the research trip to IP2I Lyon in December 2022, where the project was first discussed. AMI would also like to thank IP2I Lyon for the hospitality during several collaborative visits. The research of A.K.S is supported by the Institute Fellowship from the Indian Institute of Technology Delhi, India.

\* g.cacciapaglia@ipnl.in2p3.fr

† deandrea@ip2i.in2p3.fr

‡ iyerabhishek@physics.iitd.ac.in

§ suchita.kulkarni@uni-graz.at

¶ Abhishek.Kumar.Singh@physics.iitd.ac.in

- [1] L. Susskind, Phys. Rev. D **20**, 2619 (1979).
- [2] E. Farhi and L. Susskind, Physics Reports **74**, 277 (1981).
- [3] D. B. Kaplan and H. Georgi, Phys. Lett. B **136**, 183 (1984).
- [4] G. Cacciapaglia and F. Sannino, Journal of High Energy Physics **2014** (2014), 10.1007/jhep04(2014)111.
- [5] X. Artru and G. Mennessier, Nuclear Physics B **70**, 93 (1974).
- [6] S. B. Chun and C. D. Buchanan, Phys. Lett. B **308**, 153 (1993).
- [7] M. Grilli *et al.*, Nuovo Cim. A **13**, 593 (1973).
- [8] F. Ceradini, M. Conversi, S. D’Angelo, L. Paoluzzi, R. Santonico, and R. Visentin, Physics Letters B **47**, 80 (1973).
- [9] G. Yekutieli, S. Toaff, A. Shapira, E. Ronat, L. Lyons, Y. Eisenberg, Z. Carmel, A. Fridman, G. Maurer, R. Strub, C. Voltolini, P. Cuer, and J. Grunhaus, Nuclear Physics B **18**, 301 (1970).
- [10] E. Malaza, R. Ritchie, F. Solms, D. von Oertzen, and H. Miller, Physics Letters B **266**, 169 (1991).
- [11] V. V. Ammosov *et al.*, Phys. Lett. B **42**, 519 (1972).
- [12] M. Benedikt *et al.* (FCC), (2025), 10.17181/CERN.9DKX.TDH9, arXiv:2505.00272 [hep-ex].
- [13] C. Accettura *et al.* (International Muon Collider), (2025), arXiv:2504.21417 [physics.acc-ph].
- [14] T. A. Ryttov and F. Sannino, Phys. Rev. D **76**, 105004 (2007), arXiv:0707.3166 [hep-th].
- [15] S. Kulkarni, J. Lockyer, and M. J. Strassler, (2025), arXiv:2502.18566 [hep-ph].
- [16] K. Yamawaki, M. Bando, and K.-i. Matumoto, Phys. Rev. Lett. **56**, 1335 (1986).
- [17] M. Bando, K.-i. Matumoto, and K. Yamawaki, Phys. Lett. B **178**, 308 (1986).
- [18] T. Appelquist and Y. Bai, Phys. Rev. D **82**, 071701 (2010), arXiv:1006.4375 [hep-ph].
- [19] R. Foadi, M. T. Frandsen, and F. Sannino, Phys. Rev. D **87**, 095001 (2013), arXiv:1211.1083 [hep-ph].
- [20] T. A. Ryttov and F. Sannino, Phys. Rev. D **78**, 115010 (2008), arXiv:0809.0713 [hep-ph].
- [21] G. Cacciapaglia, C. Pica, and F. Sannino, Phys. Rept. **877**, 1 (2020), arXiv:2002.04914 [hep-ph].
- [22] R. C. Brower, A. Hasenfratz, C. Rebbi, E. Weinberg, and O. Witzel, Phys. Rev. D **93**, 075028 (2016), arXiv:1512.02576 [hep-ph].
- [23] O. Witzel, A. Hasenfratz, and C. T. Peterson (Lattice Strong Dynamics), PoS **ICHEP2020**, 675 (2021), arXiv:2011.05175 [hep-ph].

- [24] D. B. Kaplan, Nucl. Phys. B **365**, 259 (1991).
- [25] L. Vecchi, JHEP **02**, 094 (2017), arXiv:1506.00623 [hep-ph].
- [26] G. Ferretti and D. Karateev, JHEP **03**, 077 (2014), arXiv:1312.5330 [hep-ph].
- [27] G. Ferretti, JHEP **06**, 107 (2016), arXiv:1604.06467 [hep-ph].
- [28] D. B. Kaplan, H. Georgi, and S. Dimopoulos, Phys. Lett. B **136**, 187 (1984).
- [29] M. J. Dugan, H. Georgi, and D. B. Kaplan, Nuclear Physics B **254**, 299 (1985).
- [30] G. Cacciapaglia, T. Flacke, M. Kunkel, W. Porod, and L. Schwarze, JHEP **12**, 087 (2022), arXiv:2210.01826 [hep-ph].
- [31] M. Frigerio, A. Pomarol, F. Riva, and A. Urbano, JHEP **07**, 015 (2012), arXiv:1204.2808 [hep-ph].
- [32] Y. Wu, T. Ma, B. Zhang, and G. Cacciapaglia, JHEP **11**, 058 (2017), arXiv:1703.06903 [hep-ph].
- [33] C. Cai, H.-H. Zhang, G. Cacciapaglia, M. Rosenlyst, and M. T. Frandsen, Phys. Rev. Lett. **125**, 021801 (2020), arXiv:1911.12130 [hep-ph].
- [34] G. Cacciapaglia, H. Cai, A. Deandrea, and A. Kushwaha, JHEP **10**, 035 (2019), arXiv:1904.09301 [hep-ph].
- [35] H. Cai and G. Cacciapaglia, Phys. Rev. D **103**, 055002 (2021), arXiv:2007.04338 [hep-ph].
- [36] K. Agashe and R. Contino, Nucl. Phys. B **742**, 59 (2006), arXiv:hep-ph/0510164.
- [37] K. Agashe, R. Contino, L. Da Rold, and A. Pomarol, Phys. Lett. B **641**, 62 (2006), arXiv:hep-ph/0605341.
- [38] J. Alwall, M. Herquet, F. Maltoni, O. Mattelaer, and T. Stelzer, Journal of High Energy Physics **2011** (2011), 10.1007/jhep06(2011)128.
- [39] C. Bierlich, S. Chakraborty, N. Desai, L. Gellersen, I. Helenius, P. Ilten, L. Lönnblad, S. Mrenna, S. Prestel, C. T. Preuss, T. Sjöstrand, P. Skands, M. Utheim, and R. Verheyen, “A comprehensive guide to the physics and usage of pythia 8.3,” (2022), arXiv:2203.11601 [hep-ph].
- [40] L. Carloni and T. Sjöstrand, Journal of High Energy Physics **2010** (2010), 10.1007/jhep09(2010)105.
- [41] L. Carloni, J. Rathsman, and T. Sjöstrand, Journal of High Energy Physics **2011** (2011), 10.1007/jhep04(2011)091.
- [42] Pythia, “Hidden valley processes,” .
- [43] W. Liu, J. Lockyer, and S. Kulkarni, (2025), arXiv:2505.03058 [hep-ph].
- [44] R. Casalbuoni, P. Chiappetta, A. Deandrea, S. De Curtis, D. Dominici, and R. Gatto, Z. Phys. C **60**, 315 (1993), arXiv:hep-ph/9303201.
- [45] D. Buarque Franzosi, G. Cacciapaglia, H. Cai, A. Deandrea, and M. Frandsen, JHEP **11**, 076 (2016), arXiv:1605.01363 [hep-ph].
- [46] R. Caliri, J. Hadlik, M. Kunkel, W. Porod, C. Verollet, and C. Verollet, JHEP **04**, 160 (2025), arXiv:2412.08720 [hep-ph].
- [47] B. Andersson, G. Gustafson, G. Ingelman, and T. Sjöstrand, Phys. Rept. **97**, 31 (1983).
- [48] B. Andersson, G. Gustafson, and B. Soderberg, Z. Phys. C **20**, 317 (1983).
- [49] G. Cowan, K. Cranmer, E. Gross, and O. Vitells, The European Physical Journal C **71** (2011), 10.1140/epjc/s10052-011-1554-0.
- [50] B. Bellazzini, C. Csáki, and J. Serra, The European Physical Journal C **74** (2014), 10.1140/epjc/s10052-014-2766-x.
- [51] A. Agugliaro, G. Cacciapaglia, A. Deandrea, and S. De Curtis, JHEP **02**, 089 (2019), arXiv:1808.10175 [hep-ph].

SUPPLEMENTAL MATERIAL

DEPENDENCE ON LUND PARAMETERS

The discussion in the main text focused on specific multiplicities of EW-boson, whose formation from the hyper-quarks was governed by the standard QCD fragmentation function. The Lund parameters  $a_L, b_L$  were chosen to match those of QCD, fitted on available collider data. In the absence of data, not only for TC-like models but also for QCD itself at future colliders, it is important to check the robustness of the results against variation in the Lund parameters. As the  $p_T$  of the EW-bosons is an important discriminating variable for our signal, we studied the robustness of the result against changes in the fragmentation parameters. Keeping  $\Lambda_{HC} = 2$  TeV fixed, we illustrate the impact of varying  $a_L$  and  $b_L$  around the QCD value on the  $p_T$  distribution in Fig. 5. The top and bottom rows are obtained for two different values of the ratio  $\sqrt{\hat{s}_{min}}/\Lambda_{HC} = 5$  (top row) and 12.5 (bottom row). The left column corresponds to the case where  $a_L$  parameter is changed while  $b_L$  is fixed and vice versa. In each of these cases, the differences due to the respective change of the fragmentation parameters is marginal at best. Comparing the top and bottom rows reveals that substantial differences would emerge only for very high values of the ratio  $\sqrt{\hat{s}_{min}}/\Lambda_{HC}$ , which would be inaccessible at the projected energies of future colliders. As

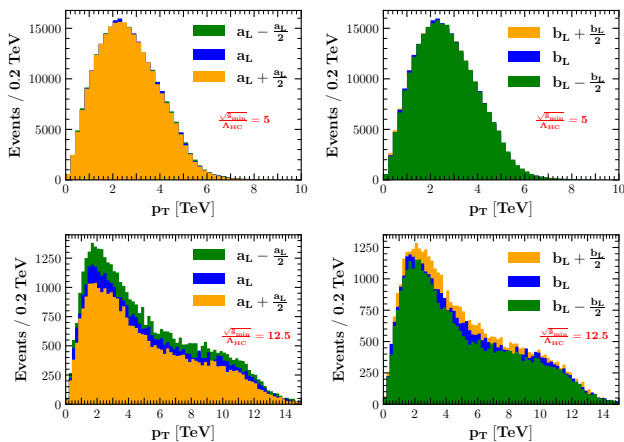


FIG. 5:  $p_T$  spectrum of the EW-bosons for different choices of the Lund parameters and  $\sqrt{\hat{s}_{min}}/\Lambda_{HC}$ . The left(right) column corresponds to the variation of  $a_L(b_L)$  while keeping the other fixed. The ratio  $\sqrt{\hat{s}_{min}}/\Lambda_{HC} = 5(12.5)$  is chosen for the top(bottom) row with  $\Lambda_{HC} = 2$  TeV.

the study will be driven by identifying EW-bosons with a given  $p_T$ , the eventual results will be largely insensitive to the uncertainties in the choice of the fragmentation

function. This observation is significant as it further ensures a broad applicability of the proposed signature to different versions of the composite models that could be governed by different confining groups and hence different values of the Lund parameters.

EFFECT OF “PROBVECTOR” ON THE FINAL STATE EW-BOSONS

The sensitivity of the results to the choice of the **ProbVector** is presented in Table II, where we compare the signal effective cross section for the value used in the main text, 0.3 as in QCD, with the value 0.75. The latter corresponds to the standard choice for the Hidden Valley (HV) module, where pions and  $\rho$  are assumed near-degenerate. As expected, the larger value of **probVector** significantly reduces the multiplicity of the pions, as it can be seen by the reduction in the 3-boson channel by a factor of 8 and the reduction by a factor of 29 in the 4-boson one.

We further illustrate this effect in Fig. 6, where we show the binned sensitivity as a function of  $\Lambda_{HC}$ , which can be directly compared with the results in Fig. 3.

probVector	3 Bosons	4 Bosons
	$\sigma_{sig}$ (ab)	$\sigma_{sig}$ (ab)
0.3	64.7	29.0
0.75	8.2	1.0

TABLE II: Comparison of signal ( $\sigma_{sig}$ ) cross sections for three and four boson final states at two different **probVector** values.

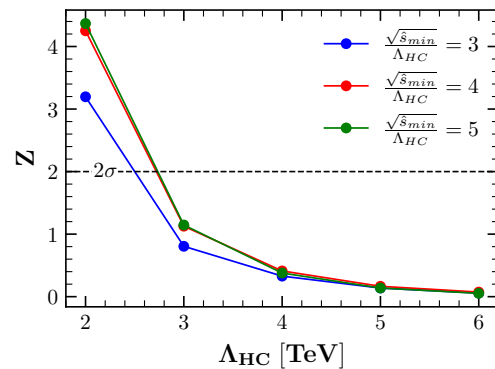


FIG. 6: Variation of the  $Z$ , signal sensitivity with  $\Lambda_{HC}$  for fixed  $\sqrt{\hat{s}_{min}}/\Lambda_{HC}$  ratio at **probVector** = 0.75.